Intense-field ionization of helium: from the UV to the static-field limit

Contact gregory.armstrong@qub.ac.uk

G. S. J. Armstrong, J. S. Parker and K. T. Taylor
Department of Applied Mathematics & Theoretical Physics, Queen's University Belfast, Belfast, BT7 1NN, UK

M. Boca
Faculty of Physics, University of Bucharest, 70709 Bucharest, Romania

Introduction

Laser–driven two-electron systems remain a challenging theoretical problem, particularly in the intense-field limit, where few simplifications of the full-dimensional time-dependent Schrödinger equation are justified. High-accuracy intense-field ionization rate calculations have a wealth of important applications. In the experimental domain, accurate rate data may help to overcome the well-known problem of determining peak laser intensities. Additionally, the full-dimensional integrations provide important guidance on the reliability of simplified theoretical models.

In [1] we presented high-accuracy calculations of single-ionization rates of helium at two optical wavelengths: 390 nm and 780 nm. We derived the intensity and frequency scaling properties of the rates in terms of simple laws derived from a ponderomotive-shifted perturbation theory. We now extend the discussion of these scaling properties with new calculations in both the high-frequency and static-field limits. The first set of calculations was performed at the 195 nm (UV) wave-length over an intensity range $0 < I < 32\times10^{14}$ W/cm^2. The second set of calculations was performed using static electric fields, with strength E in the range $0 < E < 0.4$ atomic units [2]. In both cases, single-ionization rates were obtained from the full-dimensional numerical integration of the two-electron time-dependent Schrödinger equation [3].

Figure 1 shows single-ionization rates from the $1s^2$ ground state of helium at UV and optical wavelengths, together with those for static electric fields, as a function of intensity. When plotted as $1/\ln^2$(Rate), strong linear trends become apparent. In the following sections, we derive formulae for the intensity dependence of the rates over a wide range of intensities.

Turning to the calculations of static-field ionization rates, we uncover two transition points of interest: $E = 0.175$ atomic units (au) and $E = 0.38$ au. At $E = 0.175$ au, the ionization rates undergo an abrupt change in functional form, with the sudden onset of a rapidly increasing component which scales as E^4. The electric field strength of 0.2 au is the threshold intensity for the onset of above-barrier ionization (ABI) according to Scrinzi *et al* [5]. ABI is an intense-field process in which the Coulomb potential is suppressed by the electric field, to the extent that the electron can escape above the potential barrier. As shown in figure

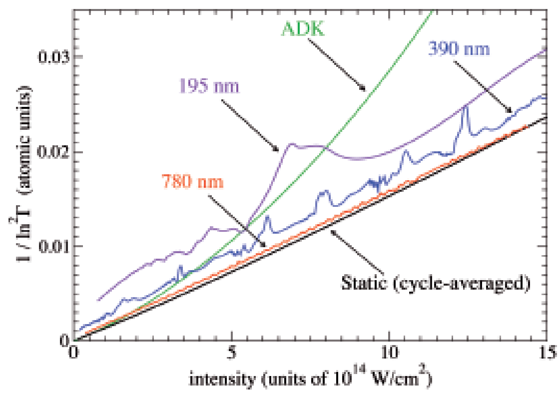

Figure 1. Numerically integrated single-ionization rates of helium. Multiphoton rates at 195 nm, 390 nm and 780 nm are shown together with cycle-averaged static-field rates, and with ADK tunneling rates.

1, the failure of the ADK tunneling formula to model the static-field ionization rate data accurately in this region is particularly pronounced. For field strengths $E < 0.38$ au, the helium atom responds adiabatically to electric fields that are ramped-on sufficiently gently. Above $E = 0.38$ au, we have difficulty producing an adiabatic atomic response for any length of ramp-on.

Ionization rate scaling laws derived from ponderomotive-shifted perturbation theory

In [1] we presented simple intensity- and frequency-scaling laws for single-ionization of helium at optical wavelengths. At the simplest level, ionization rates are given by the classic perturbation theory power law

$$\Gamma(I) = A\left(d_0^{\,2} I\right)^N . \tag{1}$$

where A is a constant, d_0 is an effective dipole moment, I is intensity in units of 10^{14} W/cm^2, and N is the number of photons required for ionization, given by I_P/ω, where I_P is the ionization potential for single-electron ionization, 0.903724 au, and ω is the laser frequency in atomic units. We now modify the ionization potential so that it incorporates the ponderomotive shift, U_P, given by $0.05336^2 I/4\omega^2$, where I is intensity in units of 10^{14} W/cm^2 (as in Wigner-Brillouin perturbation theory [4]). Our aim is to provide a simple power law, which bears out the scaling behaviour of the rates, whilst avoiding the complicated matrix elements and expansions encountered in classic perturbation theory.

In the case of the 390 nm wavelength, $\omega_{390} = 0.11683$ au, and so the number of photons required to ionize is given by $N_0(I) = (I_P + U_P)/\omega_{390} = n_{390} + \xi I$, where $n_{390} = I_P/\omega_{390} = 7.735$ and $\xi = 0.05336^2/4\omega_{390}^3 = 0.4464$. The ionization rate may then be written as

$$\Gamma(I) = A\left(d_0{}^2 I\right)^{N_0(I)}. \tag{2}$$

We then choose $A = 548000.0$ and $d_0 = 0.138$ to provide the best fit to the non-resonant trends in the 390 nm data. Figure 2 shows the predictions of equations (1) and (2) compared to the numerically integrated rates at 390 nm.

As can be seen in Figure 2, this ponderomotive-shifted perturbation theory power law works well up to an intensity of around 9.0×10^{14} W/cm^2, an order of magnitude higher than the intensities at which standard perturbation theory provides an accurate model.

Having established the success of ponderomotive-shifted perturbation theory (equation 2) at the 390 nm wavelength, we now attempt to generalize the power law, so that it may be applied at a general frequency ω, where the number of photons to ionize is given by

$$N(I) = \frac{I_p}{\omega} + \frac{0.05336^2 I}{4\omega^3}.$$

Changing units from ω to $R = \omega_{390}/\omega$, this may be written as

$$\begin{aligned} N(I) &= \left[\frac{I_p}{\omega_{390}} + \frac{0.05336^2 I}{4\omega_{390}^3}\left(\frac{\omega_{390}}{\omega}\right)^2\right]\frac{\omega_{390}}{\omega} \\ &= \left[n_{390} + \frac{0.05336^2 I}{4\omega_{390}^3}R^2\right]R. \end{aligned}$$

Henceforth, we use the scaled intensity $\bar{I} = IR^2$, so that

$$N(\bar{I}) = \left[n_{390} + \frac{0.05336^2 \bar{I}}{4\omega_{390}^3}\right]R$$

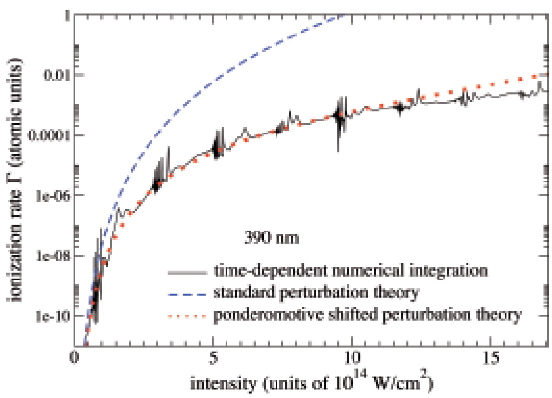

Figure 2. Numerically integrated single-ionization rates of helium at 390 nm compared to those given by equations (1) and (2).

Using the same values for the parameters A and d_0, the power law may then be recast in the form

$$\Gamma(\bar{I}, R) = \left[\frac{A}{R}\left(d_0{}^2\bar{I}\right)^{N_0(\bar{I})}\right]^R. \tag{3}$$

This formula now successfully models the 780 nm data well over the same range in I as was achieved at 390 nm[1]. At 780 nm, $R = 2$, so that the number of photons to ionize is doubled when going from 390 nm to 780 nm.

Application of scaling laws at 195 nm, 390 nm and 780 nm

The power laws of the previous section reveal the frequency scaling of the ionization rates, but several features of the rate curves in figure 1 are not directly apparent from equation (3). In particular, the vertical displacements of the rate curves from the static-field rates scale as the square of the laser frequency. Furthermore, the ordinate measure 1/(ln^2(Rate)) is nearly linear in intensity. We now introduce a new functional form for the ionization rates, which is applicable at high intensities, beyond those at which ponderomotive-shifted perturbation theory provides an accurate model of the ionization rate data. The functional form is

$$\Gamma(I, R) = \exp\left(-\frac{R}{\sqrt{a_0 + a_1 I}}\right), \tag{4}$$

which is simply an expression of the observation that 1/(ln(Rate))^2 is linear in intensity. In figures 3 to 5, the straight lines therefore correspond directly to $(a_0 + a_1 I)/R^2$.

Values of a_0 obtained from figures 3-5 are shown in table 1.

λ (nm)	Value of a_0 in figure
195	0.0009882
390	0.0009900
780	0.0009800

Table 1. Values of a_0 for each wavelength as given in figures 3 to 5.

As can be clearly seen, a_0 is largely insensitive to change in laser wavelength, and therefore the displacement between each of the rate curves, a_0/R^2, scales as the square of the laser frequency.

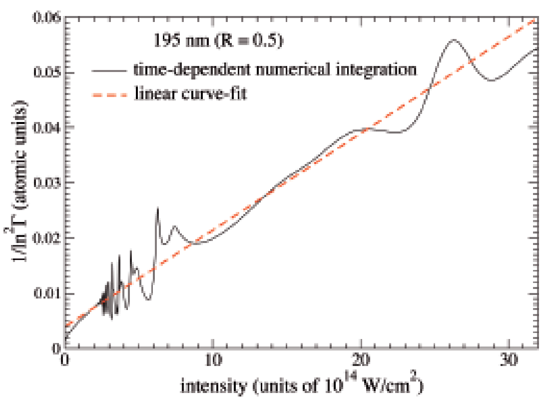

Figure 3. Single-ionization rates of helium at 195 nm as a function of intensity.

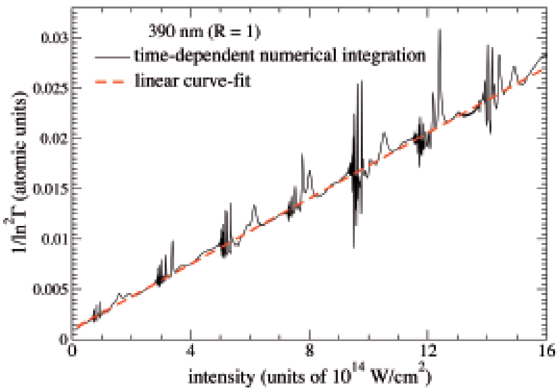

Figure 4. Single-ionization rates of helium at 390 nm as a function of intensity.

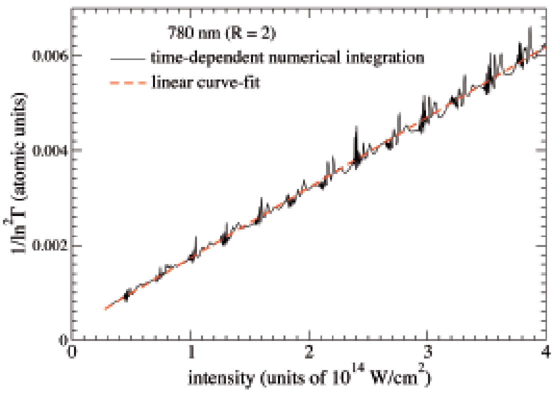

Figure 5. Single-ionization rates of helium at 780 nm as a function of intensity.

Although a_0 is insensitive to wavelength, it is sensitive to changes in ξ [2]. For example, in the $R = 1$ case, a_0 is almost linear in ξ. If ξ were half its actual value of 0.4464, then a_0 would be reduced to 0.00051. For $R = 2$, it would be reduced to 0.0006, and at $R = 0.5$ it would be reduced to 0.00038. Therefore, the vertical separation gives us a measure of the derivative of the ponderomotive shift with respect to scaled intensity, namely ξ. The frequency-squared dependence of the separation arises because the rate curves obey the familiar power law of multiphoton ionization: the minimum number of photons to ionize scales linearly with wavelength, so that R appears in the exponent. The constant ξ does not appear in the theory of static-field ionization, and so sensitivity to ξ distinguishes multiphoton ionization processes from static-field ionization processes.

We now examine the sensitivity of a_1 to change in wavelength. Table 2 shows values of a_1 obtained from figures 3 to 5.

λ (nm)	Value of a_1 in figure
195	0.001750
390	0.001630
780	0.001485

Table 2. Values of a_1 for each wavelength as given in figures 3 to 5.

Further examination of the values of a_1 shows that, to first approximation, a_1 is linear in $\ln(R)$. The smoothed ionization rates shown in figures 3-5 may be given simply as

$$\Gamma(I, R) = \exp\left(-\frac{R}{\sqrt{a_0 + a_1(R) I}}\right), \tag{5}$$

where $a_0 = 0.00099$, and

$$a_1(R) = 0.001630 + 0.000195 \ln R, \tag{6}$$

recalling that R is wavelength in units of 390 nm.

Finally, we draw attention to the fact that equation (5) fails to model the ionization rate data in the low-intensity limit. As intensity approaches zero, the rate predicted by the power law approaches zero, but the rate predicted by equation (5) does not. This feature is not so obvious in figures 4 and 5, but is clear in figure 3. In the 195 nm case, equation (5) fails to model the data accurately at intensities below 10^{14} W/cm^2.

Additionally, at sufficiently high intensities, the data departs from a linear trend in $1/(\ln(\mathrm{Rate}))^2$. At 27×10^{14} W/cm^2, the 390 nm data curls down due to the onset of a more complicated ionization process [1]. At these intensities, we observe a significant increase in population driven into doubly-excited states, which ionize less rapidly than the ground state. For this and other reasons, the rate formula presented here cannot be used to extrapolate to significantly higher intensities. The results are extended to somewhat higher intensities in [1].

Static-field ionization rates obtained using time-dependent numerical integration

In the calculation of static-field ionization rates, the time-dependent approach is advantageous, since the electric field may be ramped-on from zero to its peak value using a quarter-cycle cosine ramp-on, rather than being instantaneously switched on. The ramp-on may be made sufficiently long so as to achieve an adiabatic atomic response. More precisely, for sufficiently long ramp-on times, T, all other ramp-on times $t > T$ produce the same ionization rate. At low electric field strengths, $E > 0.08$ atomic units, a short ramp-on is generally sufficient, whereas at higher field strengths, $E > 0.3$ atomic units, a longer ramp-on is preferable. However, no adiabatic response was observed for $E > 0.38$ atomic units. In other words, each choice of ramp-on seemed to produce a different atomic response and a different ionization rate. Figure 6 shows static-

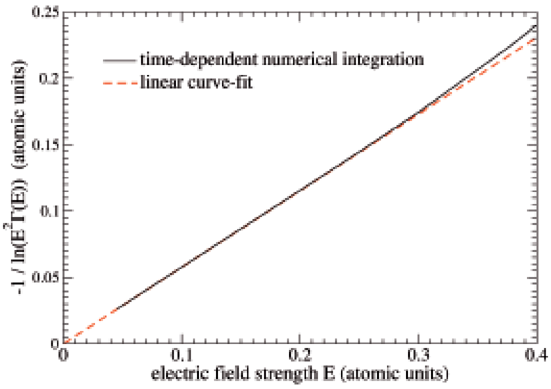

Figure 6. Single-ionization rates (-1/ln(E²Rate(E))) of helium due to static-electric fields of strength E. Rates are given in atomic units.

field ionization rates of helium. The rates are plotted as $-1/\ln(E^2\mathrm{Rate}(E))$ as a function of E.

The resulting curve is linear on the scale of figure 6 at electric field strengths below 0.2 atomic units. Above 0.25 atomic units, the onset of a new profile is clearly visible. Based on these considerations, the static-field ionization rates can be fit with a very simple function:

$$\Gamma(E) = \frac{1}{E^2}\exp\left(-\frac{1}{1.47\times 10^{-6} + 0.577E}\right) + 6.183(E-0.1755)^4\,\mathrm{Step}(E-0.1755), \tag{7}$$

where the step function, $\mathrm{Step}(x) = 1$ for $x > 0$, and 0 otherwise. Electric field strengths, E, are in the range $E < 0.4$ atomic units. Equation (7) suggests that a sudden change in the functional form of the ionization rates occurs at $E = 0.1755$, with an E^4 dependence augmenting the functional form for $E > 0.1755$.

Finally, we compare our numerically integrated ionization rates with those of time-independent calculations [4,5]. The agreement is generally good, with results typically differing by less than 2%. Furthermore, we find that the classical ADK formula fails to model the ionization rates in any limit we have considered. Its failure arises mainly from the fact that it is derived only for one-electron atoms, and in the weak-field limit.

Conclusions

We have presented high-accuracy calculations of single-ionization rates of helium at UV and optical wavelengths. We have developed accurate models for the ionization rate data in both the low- and high-intensity limits, which are equally applicable at UV and at optical wavelengths. The derived rate formulae should prove useful to experimentalists, particularly for the purpose of calibrating laser intensities.

We have also calculated static-field ionization rates of helium, and derived their dependence on peak electric field strength. The rates exhibit a tunneling-like profile for low field strengths, before suddenly departing from this behaviour at higher field strengths ($E > 0.1755$ au), where above-barrier ionization ought to be the dominant ionization process. The problem of estimating the threshold field strength for the onset of above-barrier ionization remains unsolved, despite being subject to numerous investigations [5,7-9]. Additionally, the lack of an adiabatic atomic response for $E > 0.38$ au may indicate a limit in which static-field methods fail to describe true atom-laser interactions.

Similarly, the relative contribution of tunneling is an important problem that remains poorly understood. Tunneling is a static-field process. Its magnitude is therefore bounded by the static-field ionization rates given in figure 1. It is clear from figure 1 that tunneling models, such as ADK theory, fail to provide accurate ionization rates, particularly in the high-intensity limit.

Acknowledgements

This work was supported by the UK Engineering and Physical Sciences Research Council and the Northern Ireland Department of Education and Learning.

References

1. J. S. Parker *et al.*, *J. Phys. B: At. Mol. Opt. Phys.* **40**, 1729 (2007).
2. J. S. Parker *et al.*, *J. Phys. B: At. Mol. Opt. Phys.* **42**, 134011 (2009).
3. E. S. Smyth *et al.*, *Comput. Phys. Commun.* **114**, 1 (1998).
4. Dörr *et al.*, *Phys. Rev. A* **42**, 7 (1990).
5. A. Scrinzi *et al.*, *Phys. Rev. Lett.* **83**, 706 (1999).
6. S. I. Themelis *et al.*, *Phys. Rev. A* **61**, 024101 (1999).
7. D. Bauer and P. Mulser, *Phys. Rev. Lett.* **59**, 569 (1998).
8. X. M. Tong and C. D. Lin, *J. Phys. B: At. Mol. Opt. Phys.* **38**, 2593 (2005).
9. J. Görlinger, L. Plagne and K. J. Hull, *Appl. Phys. B* **71**, 331 (2000).